Journal of Structural Geology, Vol. 9, No. 5/6, pp. 679 to 690, 1987
Printed in Great Britain

0191-8141/87 $03.00 + 0.00

Stable positions of rigid objects in non-coaxial flow—a study in vorticity analysis

CEES W. PASSCHIER

IVA, Budapestlaan 4, Utrecht, The Netherlands

(*Received* 2 *June* 1986; *accepted in revised form* 7 *March* 1987)

Abstract—Distortions of a homogeneous fabric, which occur around rigid objects in rocks deformed by non-coaxial ductile flow are useful to determine the sense of shear, but also contain information on other aspects of the flow. Rigid objects in a non-coaxial flow fall into two categories: those which are permanently rotating and those which can reach stable positions at high finite strain. The orientation of such immobilized objects with respect to eigenvectors of instantaneous flow is a function of the vorticity number of the flow, the ratio of instantaneous stretches and the axial ratio of the object. In naturally deformed rocks, immobilized rigid objects may be recognized from the geometry of the surrounding fabric. Tails of recrystallized material around porphyroclasts in a mylonite rotate towards parallellism with the extensional eigenvector of the flow, and the shape of tails reflects the rotational behaviour of the porphyroclast. The axial ratio of immobilized porphyroclasts and their orientation with respect to the tails can theoretically be used to determine the vorticity number of the flow and deviations from isochoric plane strain. In practice such an analysis is as yet difficult, but a tentative example is given of the way in which the vorticity number can be calculated from a population of feldspar porphyroclasts in a quartzite mylonite from the French Pyrenees.

INTRODUCTION

RIGID OBJECTS in rocks undergoing penetrative ductile non-coaxial flow will tend to rotate with respect to the kinematic frame of the bulk flow, and disturb the developing foliation pattern in a small adjacent domain. This disturbed pattern can be used to determine sense of vorticity of bulk flow in the rock (Simpson & Schmid 1983, Passchier & Simpson 1986). The rotational behaviour of rigid objects in a homogeneously deforming matrix is rather complex, but analytical solutions of the governing equations are known for axially symmetric objects in progressive pure or simple shear (Jeffery 1922, Bretherton 1962, Freeman 1985). Ghosh & Ramberg (1976) have shown that, even in non-coaxial flows, rigid objects of specific axial ratio will follow asymptotic movement patterns and can become stationary at high strain. If objects which have reached such stable positions can be recognized in naturally deformed rocks, their shape and orientation can provide a whole new category of information on the character and orientation of the flow pattern around them, notably on the vorticity number and the deviation from plane strain, including volume change.

This paper expands the work of Ghosh & Ramberg (1976) into a three-dimensional analysis of the nature and orientation of asymptotes for rotation of axially symmetric objects in general homogeneous steady flows, and indicates some differences between the solutions for axially and non-axially symmetric objects. Finally, I show how a population of rigid objects in a naturally deformed high-strain rock can give information on the orientation of asymptotes and, indirectly, on sense of shear and the kinematic vorticity number of the flow.

FLOW DESCRIPTION

In a body deforming by homogeneous isochoric plane-strain flow, the rate of displacement ($\dot{X}_i'$) of particles at X_i' in a fixed Cartesian co-ordinate system can be described by the velocity gradient tensor $\boldsymbol{L}'$ (Malvern 1969, p. 139) as:

$$\begin{bmatrix} \dot{X}_1' \\ \dot{X}_2' \\ \dot{X}_3' \end{bmatrix} = \begin{bmatrix} 0 & 0 & 0 \\ 0 & 0 & \frac{S+W}{2} \\ 0 & \frac{S-W}{2} & 0 \end{bmatrix} \cdot \begin{bmatrix} X_1' \\ X_2' \\ X_3' \end{bmatrix}, \qquad (1)$$

where W is the vorticity of the flow and S is a scalar defining the stretching rate of the flow (Means *et al.* 1980). $\boldsymbol{L}'$ can be expressed as the sum of a symmetric tensor $\boldsymbol{D}'$ and an antisymmetric tensor $\boldsymbol{W}'$:

$$\begin{bmatrix} 0 & 0 & 0 \\ 0 & 0 & \frac{S+W}{2} \\ 0 & \frac{S-W}{2} & 0 \end{bmatrix}_{(L')} = \begin{bmatrix} 0 & 0 & 0 \\ 0 & 0 & \frac{S}{2} \\ 0 & \frac{S}{2} & 0 \end{bmatrix}_{(D')} + \begin{bmatrix} 0 & 0 & 0 \\ 0 & 0 & \frac{W}{2} \\ 0 & -\frac{W}{2} & 0 \end{bmatrix}_{(W')}. \qquad (2)$$

The eigenvectors $\boldsymbol{d}_i$ of $\boldsymbol{D}'$ are the orthogonal instantaneous stretching axes of the flow and the eigenvalues d_1, d_2

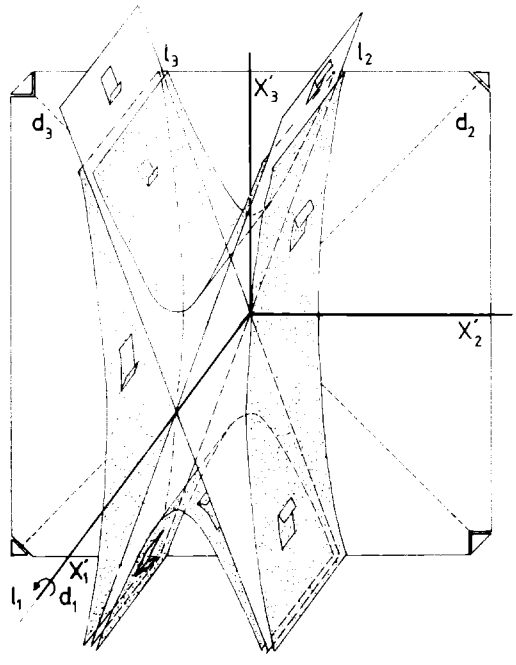

Fig. 1. Schematic representation of a homogeneous plane-strain non-coaxial flow with vorticity number $W_k = 0.76$ described by a tensor L'. X'_i—co-ordinate system. d_i—eigenvectors of D', instantaneous stretching axes. l_i—eigenvectors of L', flow apophyses. Ornamented surfaces are traced by material lines parallel to X'_1. Arrow around X'_1 indicates sense of shear.

and d_3 are instantaneous stretching rates with values 0, $S/2$ and $-S/2$. The vorticity vector of the flow is parallel to d_1 (Fig. 1).

Eigenvectors l_i of L' do not usually coincide with those of D', except for pure shear. In other cases l_1 is parallel to d_1, and l_2 and l_3 lie in the $X'_2 - X'_3$ plane symmetrically arranged with respect to d_2 and d_3 (Fig. 1) (Bobyarchick 1986, Passchier 1986). The instantaneous non-coaxiality of the flow can be expressed by a vorticity number:

$$W_k = \frac{W}{|d_2 - d_3|}, \tag{3}$$

which for isochoric plane-strain flow equals the kinematic vorticity number of Truesdell (1954):

$$W = \frac{W}{\sqrt{2\,(d_1^2 + d_2^2 + d_3^2)}}. \tag{4}$$

For pure shear $W_k = 0$, for simple shear $W_k = 1$.

The planar surfaces through l_1, l_2 and l_1, l_3, defined as eigenvector planes (Passchier 1986) have special properties for all types of instantaneous steady flow and for progressive steady flows following integration of L'. For $W_k \leq 1$ all particle paths in the flow defined by L' follow hyperboloid curves (Fig. 1) which approach the eigenvector planes asymptotically; particles within the eigenvector planes approach or depart from the X'_1 axis along paths within the planes. For these reasons, eigenvectors l_2 and l_3 have been named flow apophyses by Ramberg (1975a, b). For plane-strain flow, particle paths within the eigenvector planes are the only straight orbits in the flow (Fig. 1).

MOVEMENT OF AXIALLY-SYMMETRIC RIGID OBJECTS

General theory—isochoric plane-strain flow

Governing equations of the movement of rigid objects in homogeneous flow (Jeffery 1922, Bretherton 1962, Gierszewski & Chaffey 1977, Hinch & Leal 1979, Freeman 1985) are least complex for axially symmetric ellipsoidal objects. The axial ratio of such objects can be expressed by a component B of the Bretherton shape tensor (Bretherton 1962), where a is the length along the symmetry axis and b the radius in the circular section (Fig. 2):

$$B = \frac{a^2 - b^2}{a^2 + b^2}. \tag{5}$$

Thus B can represent a material line ($B = 1$), a prolate ellipsoid ($0 < B < 1$), a sphere ($B = 0$), an oblate ellipsoid ($-1 < B < 0$) or a material plane ($B = -1$). If an internal reference frame X_i is chosen with X_1 fixed to the object symmetry axis (OSA), the rotation of the object with respect to the external reference frame X'_i is given by the Eulerian angles θ, ϕ and ψ, described by a rotation tensor $\boldsymbol{R}$ (Goldstein 1980, p. 147). However, the orientation of an axially symmetric object can be defined by two angles only: in this paper $\theta = 90°$ which reduces ϕ to the azimuth and ψ to the plunge of the OSA (Fig. 2a). $\boldsymbol{D}'$ and $\boldsymbol{W}'$ can now be expressed in terms of the internal reference frame by:

$$\boldsymbol{D} = \boldsymbol{R}\boldsymbol{D}'\boldsymbol{R}^{\mathrm{T}} \tag{6}$$

and

$$\boldsymbol{W} = \boldsymbol{R}\boldsymbol{W}'\boldsymbol{R}^{\mathrm{T}}. \tag{7}$$

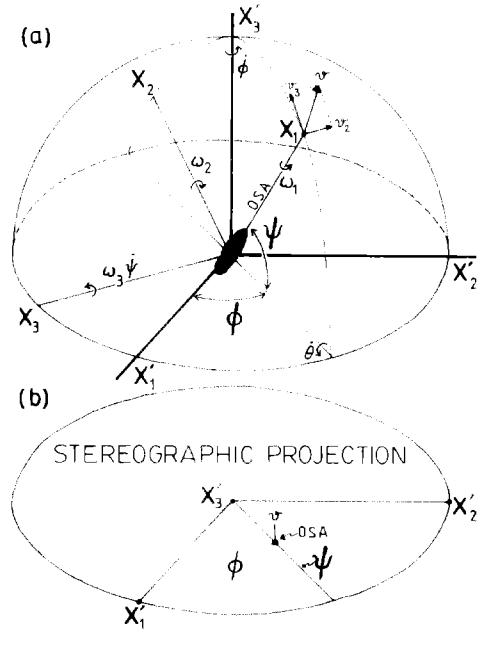

Fig. 2(a). Reference frame for rotation of axially symmetric rigid ellipsoids. X'_i and X_i—external and internal co-ordinate systems. ϕ and ψ—azimuth and plunge of object symmetry axis (OSA). ω_i—angular velocity components of OSA around X_i. θ, ϕ, $\dot{\psi}$—rate of change of Eulerian angles. ν—instantaneous displacement rate of OSA on a sphere around centre of co-ordinate systems. (b) Stereographic projection of OSA and ν.

The instantaneous angular velocities of the object around the X_i axes are now (Freeman 1985):

$$\omega_1 = -W_{32} = \frac{S\,W_k}{2}\cos\phi\cos\psi,$$

$$\omega_2 = -W_{13} - BD_{32} = \frac{BS - W_k\,S}{2}\cos\phi\sin\psi, \quad (8)$$

$$\omega_3 = -W_{21} + BD_{21} = \frac{S}{2}\sin\phi\,(W_k + B\cos 2\psi).$$

Here ω_1 describes the axial rotational velocity of the object around its symmetry axis, zero if the OSA lies in the $X_2' - X_3'$ plane and a maximum if it lies parallel to X_1'; ω_2 and ω_3 describe the angular velocity of the OSA with respect to X_i and can be recalculated in terms of $\dot\theta$, $\dot\phi$ and $\dot\psi$, the rates of change of Eulerian angles in the external reference frame X_i':

$$\dot\theta = -\omega_2\sin\psi,$$
$$\dot\phi = \omega_2\cos\psi, \quad (9)$$
$$\dot\psi = \omega_3.$$

In order to understand how W_k, B, ϕ, ψ and S influence the movement pattern of objects, the instantaneous displacement rate of the OSA along a sphere around the centre of the co-ordinate systems was calculated from equations (8) for a number of OSA positions and plotted as a vector v in stereograms (Figs. 2 and 3). S appears as a constant in all equations (8) and its magnitude does not influence the shape of the flow patterns: in the calculations a value $S = 10$ was used. A half stereogram is sufficient for presentation of the movement pattern because of its bilateral symmetry.

The vectors in Fig. 3 describe the *instantaneous* movement of the OSA, but the vector field traces a regular pattern which defines potential finite trajectories of the OSA in steady flows, as obtained by numerical integration of equations (9) (e.g. Freeman 1985). OSA-trajectories for $S = 10$ have been constructed from stereograms (as in Fig. 3) for a complete range of B and W_k values (Fig. 4). It is clear that both B and W_k have a profound influence on the shape of the OSA trajectories. All patterns have complete bilateral symmetry on the $X_2' - X_3'$ plane and two extra mirror planes for the shape of OSA trajectories only. Some of the patterns contain 'stable positions' at which an OSA would remain immobile during progressive deformation provided that B, W_k and the orientation of the kinematic frame of flow do not change. These stable positions fall into three categories: *sources* at which the OSA are in metastable equilibrium; *sinks* at which the OSA are in stable equilibrium; *transient positions* where small deviations from these points can cause a return of the OSA or a permanent removal depending on the direction in which the deviation operates. Outside the stable positions the OSA accelerate and decelerate along simple paths either to reach a sink or transient stable position, or to rotate permanently along the same orbit (Jeffery 1922, Bretherton 1962, Hinch & Leal 1979). The patterns can

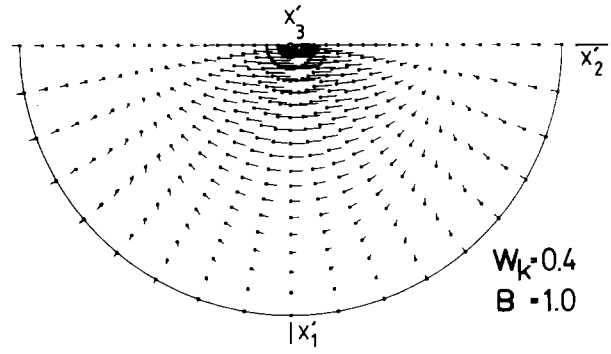

Fig. 3. Computer-generated upper hemisphere Wulff projection of displacement rate vectors of OSA at 343 positions. 10° intervals of ϕ and 5° intervals of ψ. $W_k = 0.4$, $B = 1.0$.

be subdivided according to B and W_k values as follows (Fig. 4).

(a) $W_k < |B|$. Three stable positions exist in the diagrams: a transient position parallel to X_1' and a source–sink pair in the $X_2' - X_3'$ plane. Source and sink are always symmetrically arranged with respect to d_i, and their actual positions depend on the sense of vorticity, B and W_k. At $W_k = 0$ (pure shear) source and sink coincide with eigenvectors of D' and L' at 45° to X_2' and X_3' (Fig. 4). For any W_k, material lines ($B = 1$) follow a trajectory towards a sink parallel to l_2, and the normal to material planes ($B = -1$) approaches a sink normal to l_2. The OSA of objects with other B-values have a source and sink at an angle $\pm\,\beta/2$ from X_3' (Fig. 4) defined by:

$$\cos\beta = \frac{W_k}{B}. \quad (10)$$

(b) $W_k = |B|$. A 'stable plane' exists through X_1' and X_3' ($B > 0$) or X_2' ($B < 0$). All OSA within this plane are in transient equilibrium. Outside the stable plane OSA rotate along straight planar paths towards X_3' or X_2'. If $W_k = 1$, the stable plane coincides with the neutral or shearing plane of simple shear flow.

(c) $W_k > |B|$. Only a transient position exists along X_1'. In all other positions the OSA rotate continuously along closed Jeffery orbits (Jeffery 1922, Freeman 1985). The same effect occurs if $B = 1$ or -1, but $W_k > 1$: in other words, if the flow contains a component of rigid body rotation in the external reference frame (Ramberg 1975b, Means *et al.* 1980).

General flow

For non-isochoric non-plane strain, the rotational behaviour of axially symmetric objects is more complex than that outlined above. The components of L' are now:

$$L' = \begin{bmatrix} d_1 & 0 & 0 \\ 0 & \dfrac{d_2 + d_3}{2} & \dfrac{d_2 - d_3 + W}{2} \\ 0 & \dfrac{d_2 - d_3 - W}{2} & \dfrac{d_2 + d_3}{2} \end{bmatrix}. \quad (11)$$

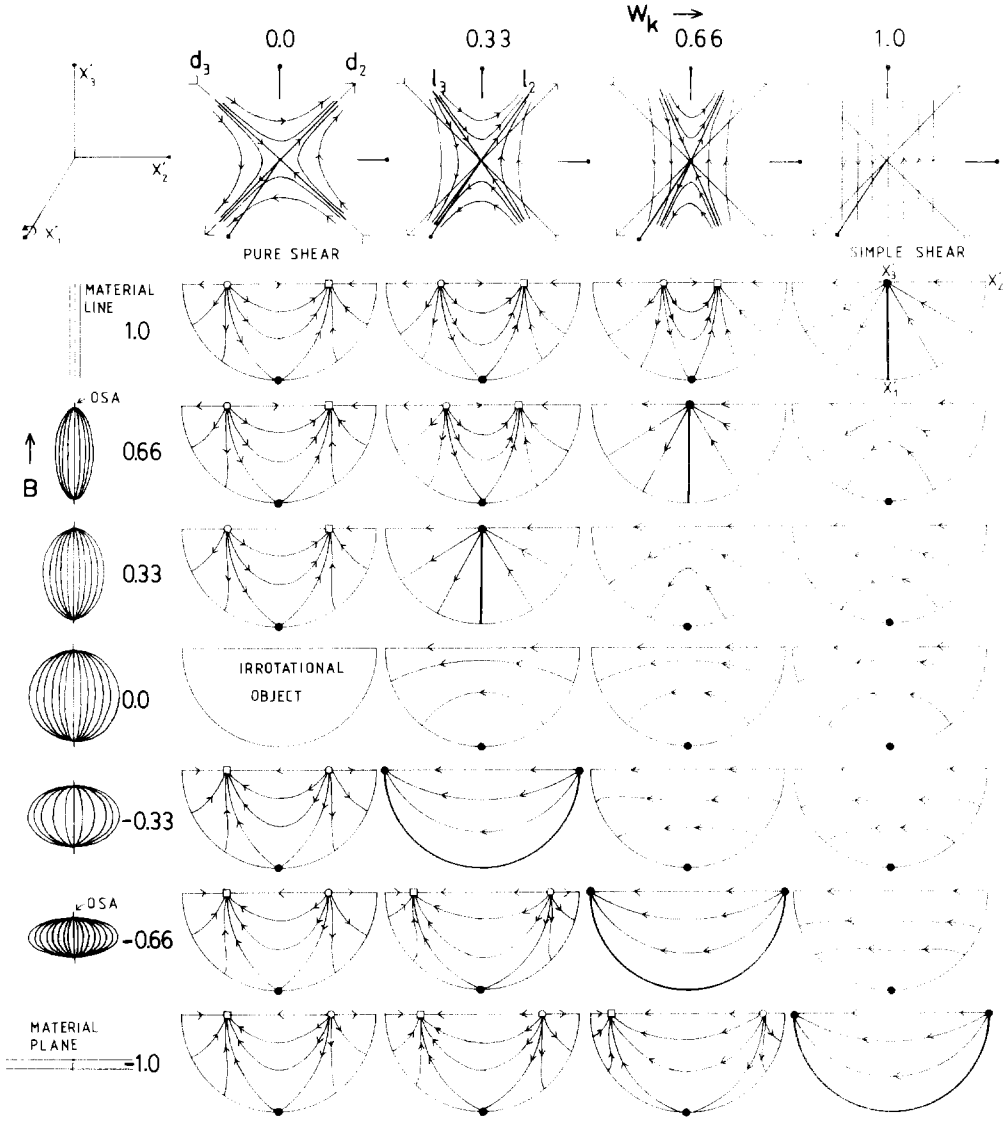

Fig. 4. Movement patterns of the object symmetry axis (OSA) for the range of possible W_k and B values. Upper hemisphere Wulff projection. Representative flow types shown along the top, representative object shapes on the left. Symbols in stereograms: open circles—sources of OSA; open squares—sinks of OSA; solid circles—transient stationary positions of OSA; bold lines at $W_k = |B|$—planes of transient stable positions. d_i—eigenvectors of D' (instantaneous stretching axes). l_i—eigenvectors of L'.

This tensor description can be used to obtain the following equations for angular velocities around the OSA in the same way as described above:

$$\omega_1 = \frac{W}{2}\cos\phi\cos\psi,$$

$$\omega_2 = -\frac{\cos\phi}{2}\{W\sin\psi + B(2d_1 - d_2 - d_3)\cos\psi \times \sin\phi - B(d_2 - d_3)\sin\psi\}, \quad (12)$$

$$\omega_3 = \frac{1}{2}\{W\sin\phi - B(2d_1 - d_2 - d_3)\sin\psi\cos\psi \times \cos^2\phi + B(d_2 - d_3)\sin\phi\cos 2\psi\}.$$

The conditions at which the OSA is stationary in general flow types can be found by solving equations (12) for $\omega_2 = \omega_3 = 0$. Elimination of ϕ and ψ gives:

$$V^2 = \frac{B^2 - W_k^2}{B^2}, \quad (13)$$

where V is defined as:

$$V = \frac{2d_1 - d_2 - d_3}{d_2 - d_3}. \quad (14)$$

It can easily be shown from equations (12) that equation (10) is valid for general flow types as described above and thus follows from equation (13):

$$V = \sin\beta. \quad (15)$$

Movement patterns of the OSA in general flow types, as defined by equations (11) and (12), can be grouped into specific fields in $B - W_k - V$ space, whose boundaries are defined by equations (13) and (15). The patterns have the following properties (Fig. 5; only positive B values described, for simplicity).

(a) If $V \neq 0$, movement patterns lack orthorhombic symmetry but are always bilaterally symmetric.

(b) If $V = 0$, movement patterns are identical to

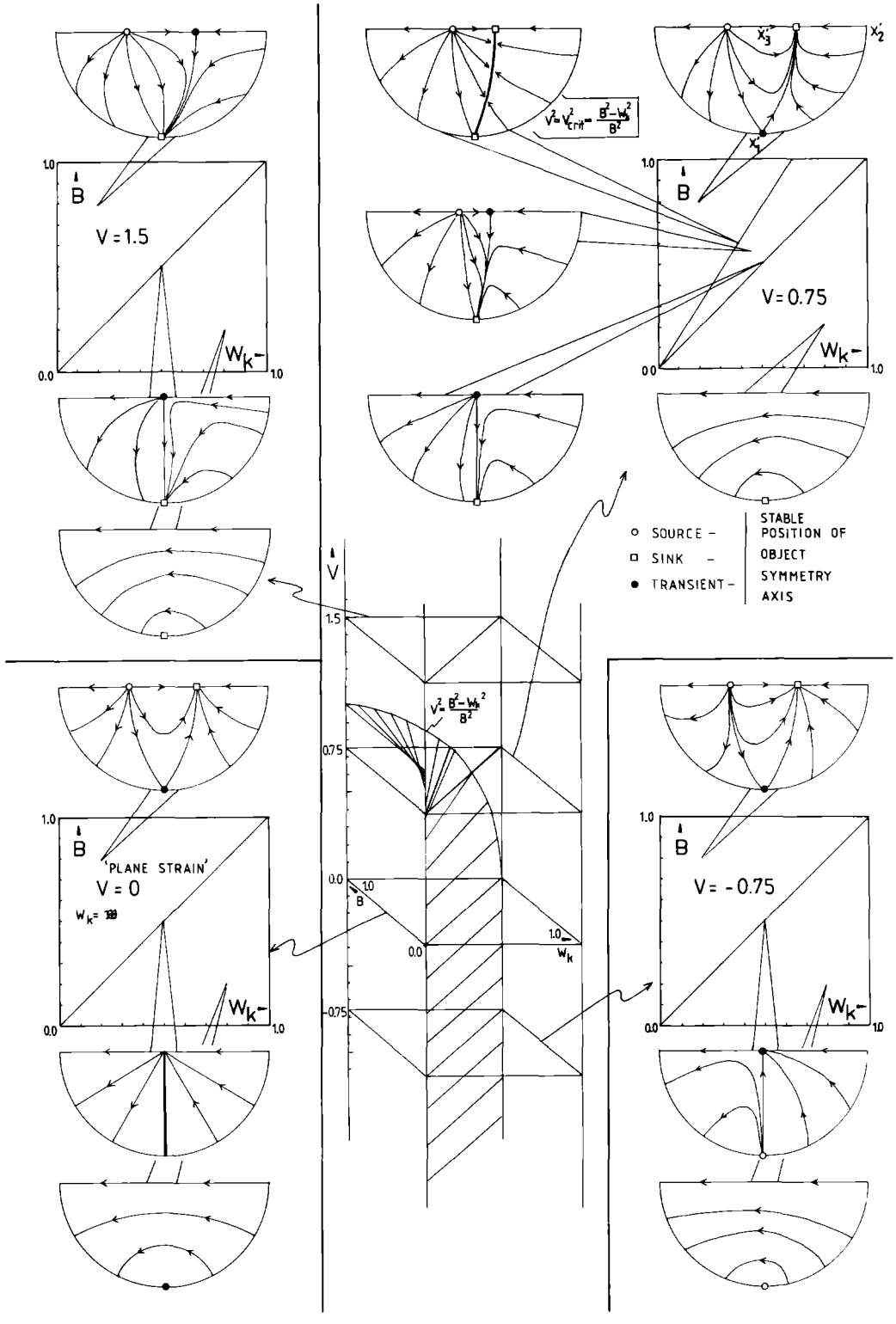

Fig. 5. Movement patterns of the object symmetry axes (OSA) for general flow types. The central column shows subdivision of V–W_k–B space into domains with different types of movement patterns. Four levels (V = −0.75, 0.0, 0.75 and 1.5) show the full range of possible patterns. Symbols in stereograms as in Fig. 4. Further explanation in text.

those of Fig. 4. Isochoric plane strain flow is one of the possible regimes in this category.

(c) If $V < 0$, as for constrictional flow, a drift of the OSA towards the $X_2' - X_3'$ plane is superimposed on the plane strain patterns. If $W_k > B$, the OSA moves in spirals towards the $X_2' - X_3'$ plane, except if it already lies in this plane in which case it rotates permanently in a closed orbit. The number of rotations needed to reach the $X_2' - X_3'$ plane is a function of V. If $W_k = B$ the OSA approaches a transient position parallel to X_3' after one orbit (Fig. 5). If $W_k < B$, a sink–source pair is present in the $X_2' - X_3'$ plane, separated by the same angle β as for similar W_k and B values in isochoric plane strain flow: however, actual movement paths differ in both flow types. This also applies under certain conditions if $V > 0$ (see below).

(d) If $V > 0$, as for flattening flow, the situation is much more complex. If $W_k > B$, all OSA except those in the $X_2' - X_3'$ plane follow spiralling paths towards X_1', which acts as a sink. If $W_k = B$, the same happens along more complex orbits, and a transient position exists along X_3'. If $W_k < B$, the extension parallel to X_1' counteracts the drift of OSA towards a sink in the $X_2' - X_3'$ plane. The actual pattern of stable positions depends on the ratio W_k–B–V. If $0 < V < 1$ and

$$\frac{B^2 - W_k^2}{B^2} < V^2 \quad \text{or} \quad \sin\beta < V, \tag{16}$$

objects will approach the sink in the $X_2' - X_3'$ plane, but less rapidly than for plane strain and along a narrow corridor which follows a great circle between the sink and X_1'. If

$$\frac{B^2 - W_k^2}{B^2} > V^2 \quad \text{or} \quad \sin\beta > V, \tag{17}$$

the sink in the $X_2' - X_3'$ plane is changed to a transient position and a sink is created along X_1' (Fig. 5). If equations (13) or (15) are satisfied, all OSA travel along paths from the source on the $X_2' - X_3'$ plane towards a *sink-plane* through X_1'. Consequently, a transient position along X_1' and a sink in the $X_2' - X_3'$ plane, as for isochoric plane strain flow, only exist if the B–W_k–V co-ordinates of the flow can be plotted below the ornamented surface in the central column of Fig. 5.

AXIALLY NON-SYMMETRIC OBJECTS

The rotational behaviour of objects with general orthorhombic shape symmetry is incompletely understood since governing equations need numerical solution. However, the theory of existing sink positions for certain W_k values and object shapes does not break down for objects which lack axial symmetry. For an object with a, b and c axes parallel to X_1, X_2 and X_3 ($c > a > b$), the rotational behaviour in isochoric plane strain can be derived as outlined above and in Freeman (1985);

$$\begin{aligned}
\omega_1 &= \frac{S}{2}\{\cos\psi\cos\phi\,(W_k + B_1\cos 2\theta) \\
&\quad - \sin\psi\sin\phi\cos\theta\,(W_k + B_1)\}, \\
\omega_2 &= \frac{S}{2}\{\cos\psi\sin\phi\cos\theta\,(B_2 - W_k) \\
&\quad + \cos\phi\sin\psi\,(B_2\cos 2\theta - W_k)\}, \\
\omega_3 &= \frac{S}{8}\{4\sin\phi\sin\theta\,(W_k + B_3\cos 2\psi) \\
&\quad + B_3\sin 2\psi\sin 2\theta\cos\phi\},
\end{aligned} \tag{18}$$

in which

$$B_1 = \frac{b^2 - c^2}{b^2 + c^2}, \quad B_2 = \frac{c^2 - a^2}{c^2 + a^2}, \quad B_3 = \frac{a^2 - b^2}{a^2 + b^2}. \tag{19}$$

From (18) the equations for $\dot{\theta}$, $\dot{\phi}$ and $\dot{\psi}$ of object axes in the external reference frame can be calculated. For axially non-symmetric objects, the angular velocity of the longest or shortest axis of the object is not only a function of its orientation in the flow, as for axially symmetric objects, but also of the orientation of the other two symmetry axes. For objects which deviate slightly from axial symmetry (e.g. with axial ratios of 10:5:4), two stable sink positions can be found in the $X_2' - X_3'$ plane, depending upon whether the shortest or the intermediate axis is parallel to X_1' (Fig. 6). The orientation of these sink positions can be found using an equation similar to (10):

$$\cos\beta = \frac{W_k}{B^*}, \quad B^* = \frac{Mx^2 - Mn^2}{Mx^2 + Mn^2}, \tag{20}$$

where Mx and Mn are the object's long and short symmetry axes in the $X_2' - X_3'$ plane. Two sources exist in this plane diametrically opposite the sinks from X_3'. Numerical solution of equation (18) for some object orientations shows that the object's longest axis migrates from any orientation in the flow towards the general area of the two sinks (Fig. 6), provided:

$$W_k < B_2. \tag{21}$$

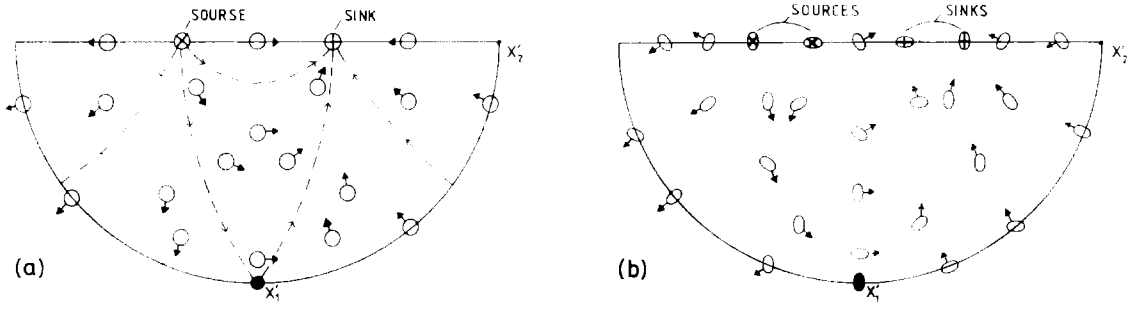

Fig. 6(a). Instantaneous displacement directions of the symmetry axis of axially symmetric prolate objects along a sphere for non-coaxial flow with $W_k < B$. One source–sink pair exists for this axis. Most movement directions trace orbits towards the sink, some towards the transient stable position (solid circle). (b) Instantaneous movement directions of the longest axis of a prolate object with orthorhombic symmetry along a sphere for $W_k < B_2$. Two source–sink pairs exist for the long axis, active when either the shortest or the intermediate axis of the object lies parallel to X_1'. Instantaneous movement direction of the longest axis depends on the general orientation of the ellipsoid, indicated by the orientation of an ellipse in the diagram; most long axes trace orbits towards the sink pair and some towards the transient position (solid ellipse). Upper hemisphere Wulff projections.

Only the initial orientation of the short and intermediate symmetry axes determine the actual movement path towards the sinks.

PRACTICAL APPLICATION

Introduction

Rigid objects suspended in any homogeneous viscous non-coaxial flow can be divided into two groups: those with permanently rotating symmetry axes and those which can reach a stable sink position in the $X_2' - X_3'$ plane of the flow. Objects of the second group become immobilized with one symmetry axis parallel to X_1' and two symmetry axes in the $X_2' - X_3'$ plane, one of which is at the actual sink position. Such objects are totally immobile since ω_1, ω_2 and ω_3 are all zero [equations (8), (12), (18)]. Equation (20) describes the orientation of the symmetry axis at the sink position with respect to X_3' for immobilized objects of general orthorhombic shape as a function of B^* and W_k only. Axially non-symmetric objects can have two sink positions of a symmetry axis in the $X_2' - X_3'$ plane (Fig. 6) but for each of them equation (20) applies. Although the actual path to reach a stable sink position in the $X_2' - X_3'$ plane depends on W_k, V and B_i, the orientation and length–width ratio of the cross-section in the $X_2' - X_3'$ plane of any immobilized object can be used to calculate B^* and β or some function of these values, and thus W_k. This applies for any steady, homogeneous flow and additional information on the 3-D shape and orientation of the object places further constraints on the nature of the flow. These principles are of great interest to geologists although practical applications are as yet wrought with difficulties.

Application to rocks

In a sample of deformed rocks it is difficult to determine which objects had reached a stable position, and which were still rotating as deformation stopped. Rigid porphyroclasts in a ductilely deforming matrix often recrystallize along their margins and produce tails of fine recrystallized material which stretch out into the matrix. Immobile objects with a symmetry axis at a sink in the $X_2' - X_3'$ plane of the flow can be expected to show straight σ-type tails with 'stair-stepping' (Fig. 7) (Passchier & Simpson 1986). Permanently rotating objects tend to deform the developing tails in a more or less complex manner. Ellipsoidal objects rotate by periodic accelerations and decelerations (Fig. 3) which also influence recrystallization rates. Tail development will be significant during the period of slow rotation when the long axes of the object are near the $X_1' - X_3'$ plane, and these tails will become distorted to δ-types during the subsequent fast rotation when the long axes are near the $X_1' - X_2'$ plane (Fig. 7). In this way, each 180° rotation can produce its own set of tails and complex porphyroclast-tail systems will develop (Fig. 7 and Passchier & Simpson 1986). δ-type tails can also develop around spherical rotating objects if recrystallization is slow. Thus, complex and δ-type clast–tail systems are considered to be indicative of permanently rotating objects, while objects with straight σ-type tails are probably at stable positions.

Tails of recrystallized material will tend to rotate towards the extensional eigenvector l_2 of L' throughout the deformation. For deformation histories in which l_2 does not rotate systematically through the material, recrystallized tails will reach parallelism with l_2 at high finite strains. The angle η between the Mx-axis of an irrotational rigid object, which lies at a sink in the $X_2' - X_3'$ plane, and l_2 or the straight domain of the tail away from the object is a function of W_k and B^* only:

$$\eta = \frac{1}{2}\sin^{-1}\frac{W_k}{B^*}\{\sqrt{1 - W_k^2} - \sqrt{B^{*2} - W_k^2}\}.$$

Figure 8(a) gives a plot of η for the entire range of possible W_k and B^* values. η increases with decreasing B^* up to the value $B^* = W_k$, the 'cut-off point'. At still lower B^* values, the objects are rotating permanently. W_k can be derived from these graphs in two ways (Fig. 8b): (a) from the value

$$B^*_{crit} = W_k,$$

which separates the σ-type immobilized part of the clast

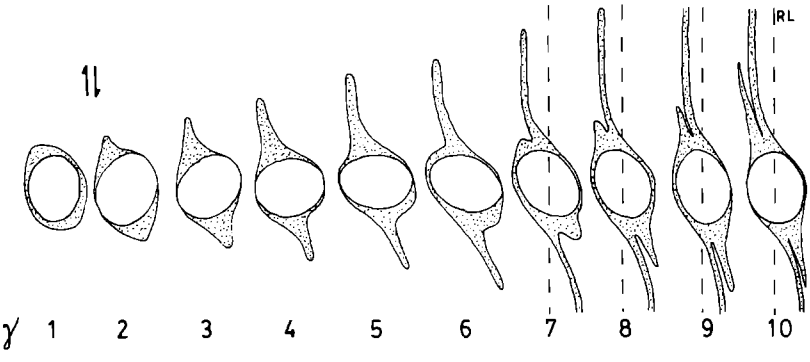

Fig. 7. Schematic reconstruction of the development of complex tails of recrystallized material around a rigid ellipsoidal object in simple shear, based on shearbox experiments. σ-type tails of recrystallized material, generated when the object's long axis lies near the flow plane (γ = 1–2) are deformed to δ-type tails (γ = 3–6), followed by generation of new tails of σ-type (γ = 7–10). Cross-sections normal to the vorticity vector.

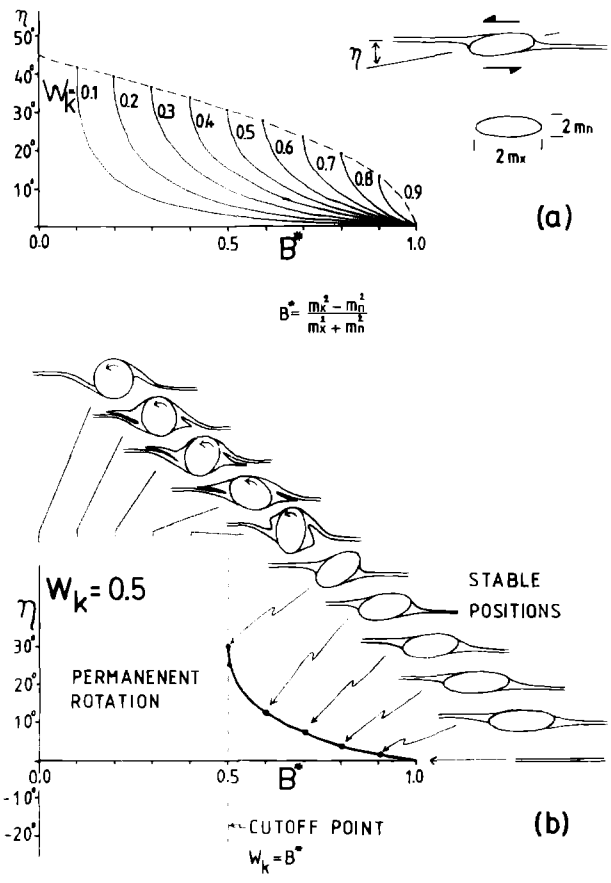

Fig. 8(a). Curves for the orientation of stable sink positions of rigid objects in the $X_2' - X_3'$ plane of flow for a range of W_k values. η—angle between the long axis of an object cross-section and l_2, marked by recrystallized tails at high finite strain. B^*—shape factor. If $W_k > B^*$ no stable sink positions exist. (b) Example of the expected geometries of rigid-object recrystallized tail systems in cross-section parallel to $X_2' - X_3'$ at $W_k = 0.5$. At low B^* values, objects rotate permanently and generate δ-type and complex tails. At high B^* values, to the right of the 'cutoff point', objects have their long axis at a stable sink position and generate σ-type tails only. η decreases with increasing B^*.

population in a rock from the complex and δ-type rotational part, and (b) theoretically from η and B^* for individual objects if subparallellism of recrystallized tails with l_2 during the last stages of the flow can be proven.

As a first attempt to apply the theory to rocks, the following five requirements should at least be met. (1) The fabric and general setting of the samples should indicate that deformation was reasonably homogeneous on the scale of the sample and that systematic changes in the orientation of the kinematic frame of the flow are unlikely due to the regional setting. Samples from the limb of a major fold are unsuitable, but samples from a straight, regular shear zone may be useful. (2) Grain size in the matrix should be significantly smaller than the size of the objects in order to make reasonable the assumption of homogeneous flow. (3) High finite strains accumulated by homogeneous flow are required to rotate sufficient objects towards sink positions. (4) Object shape should be regular and closely approach orthorhombic shape symmetry. Deviations of object shape from an ellipsoid are not expected to influence the position of sinks (Bretherton 1962). (5) A sample should contain a large number of spatially well dispersed objects with variable B^* values.

Mylonite sample

In mylonites produced by homogeneous non-coaxial flow leading to high finite strains, porphyroclasts with high B^* values can be expected to reach stable sink-positions. Such clasts should be recognizable from their tail geometry and from a preferred orientation of one of the OSA parallel to the vorticity vector of the flow.

A sample of quartzite mylonite from the St. Barthelémy Massif, French Pyrenees, has been used for an analysis of porphyroclast orientation. The sample was taken from a planar quartzite lens in a major shear zone. The surrounding mylonitic gneiss contains a planar mylonitic shape fabric formed under upper-greenschist facies conditions (Passchier 1985). The quartzite mylonite has a matrix of weakly elongate dynamically recrystallized quartz grains (20 μm average grain size) which define an oblique foliation. Numerous isolated porphyroclasts of K-feldspar lie in the matrix with elongate straight recrystallized tails, defining a good stretching lineation and compositional layering at an angle of 28° to the quartz fabric. No boudinage or sheath-folding of the compositional layering was observed, and the quartz fabric does not change in character and orientation towards the recrystallized feldspar tails: this suggests that the tails approached passive-marker behaviour in the flow. All clast-tail systems show consistent stair-stepping symmetry indicating non-coaxial flow (Fig. 9). R_f in the sample must exceed 500 judging by the length–width ratio of recrystallized feldspar tails (Fig. 9). The homogeneity of preferred orientation patterns of quartz (both crystallographic and shape) throughout the sample suggests that the flow which produced them was reasonably homogeneous on sample scale. The transparent nature of the quartzite allows observation of the complete 3-D geometry and orientation of porphyroclast–tail systems in 1 mm thick sections parallel to the stretching lineation and normal to the foliations; i.e. in the inferred $X_2' - X_3'$ plane of the flow (e.g. Simpson & Schmid 1983, Passchier & Simpson 1986).

Most porphyroclasts in the sample are oblate. Prolate clasts usually have their long axes in the plane of the thin section. In cross-section parallel to this plane, complex (Fig. 9a), δ-type and apparently immobilized σ-type clasts (Fig. 9b) are all present. All porphyroclasts with approximately orthorhombic shape symmetry and two symmetry axes in the plane of the section were analysed as follows: B^* values in the inferred $X_2' - X_3'$ plane and η, the angle between the long axis and the trace of the tail away from the clast, were measured and plotted (Fig. 10). Because of the high inferred finite strain values, the tails are assumed to parallel l_2, at least during the last stages of deformation. Objects smaller than 100 μm were omitted from the analysis because flow cannot be expected to have been homogeneous on this scale. Nearly all complex and δ-type clast–tail systems (open circles) plot left of the $B^* = 0.6$ line. A dense cluster

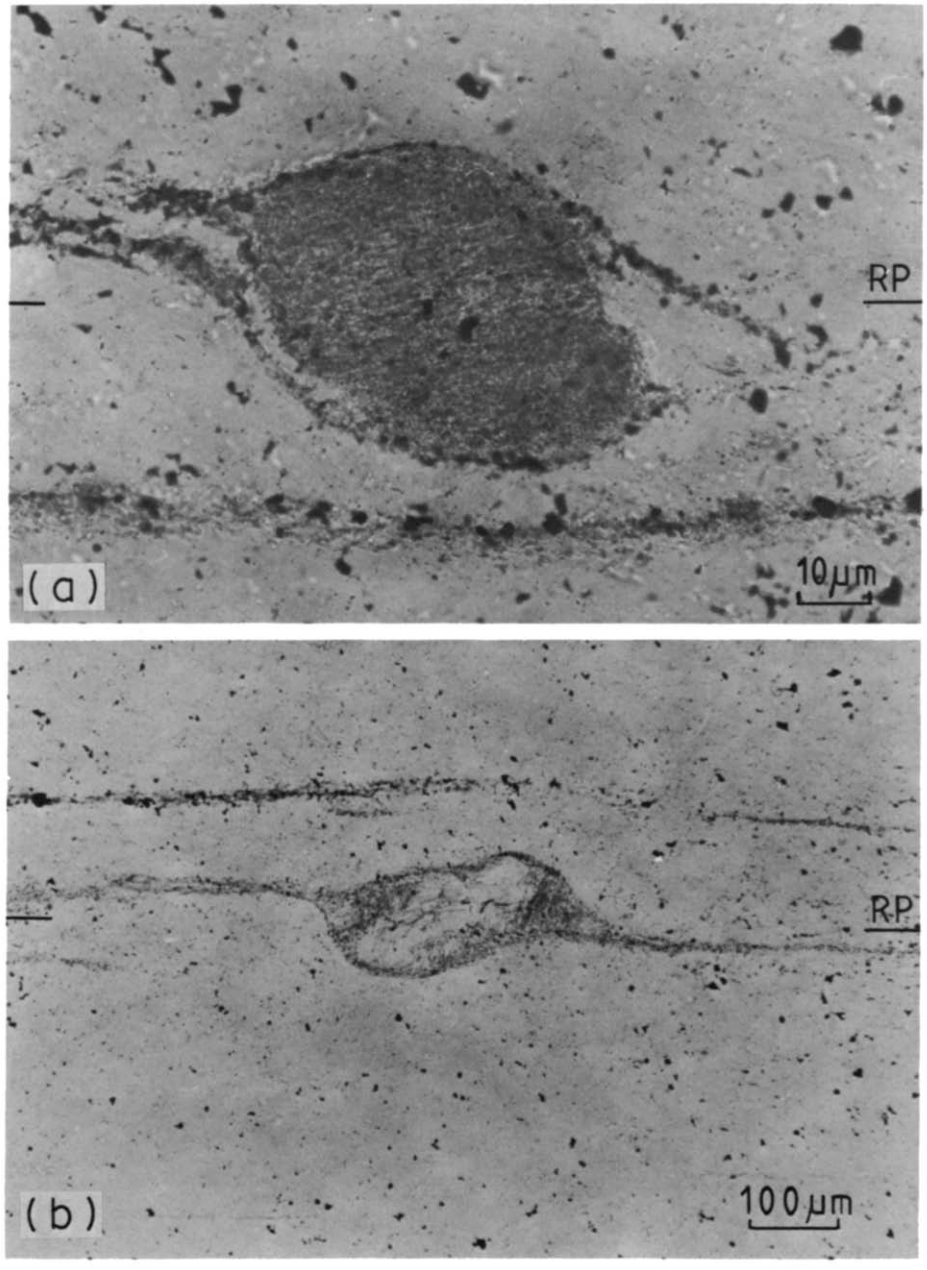

Fig. 9. Porphyroclasts of K-feldspar with fine-grained recrystallized tails in quartzite mylonite, St. Barthélemy Massif, France. Stair stepping of recrystallized tails with respect to reference plane (RP) from right to left indicates sinistral sense of shear. (a) Complex clast–tail system indicative of permanent rotation, $B^* = 0.38$; (b) σ-type clast–tail system ($B^* = 0.76$) in which the clast is inclined in opposite direction to the stair stepping of tails, probably indicating that the object's long axis was near a stable sink position.

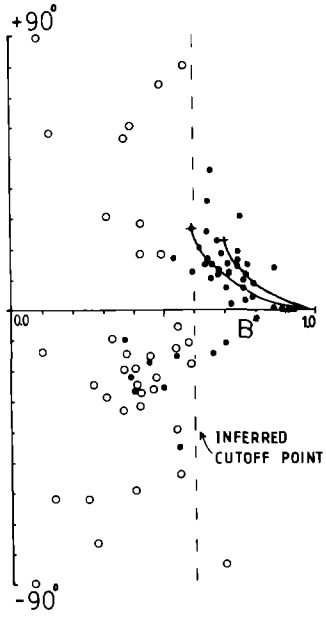

Fig. 10. Data plot of K-feldspar clast-tail systems in quartzite mylonite, St. Barthélemy Massif, France, from thin sections normal to the inferred vorticity vector of the flow. Orientation of object long axes with respect to trace of recrystallized tails, in degrees, plotted against B^*, as in Fig. 8. Open circles, clast–tail systems with complex or δ-type geometry indicative of permanent rotation; dots, σ-type clast–tail systems. Further explanation in text.

of σ-type systems (dots), which dip in the opposite direction to the stair stepping, plot to the right of this line. The solid curves (Fig. 10) represent theoretical η values for $W_k = 0.6$ and 0.7 from Fig. 8. As would be expected for naturally deformed rocks with non-axially symmetric objects, there is no close fit of data points to a specific curve, but a cluster in the general region certainly exists. Scattering can be due to: (a) fluctuations of non-axially symmetric objects in between their two sink-orientations; (b) changes in B^*-values of objects with progressive deformation due to recrystallization without instant reorientation of the object; and (c) the probability that recrystallized tails did not act as perfectly passive markers. Figure 10 suggests that the flow which produced the fabric in this sample was not simple shear, but had a W_k number between 0.5 and 0.8, possibly 0.6. The general dominance of the long axes of prolate objects in the inferred $X_2' - X_3'$ plane seems to indicate that $V \leq 1$ and that observations lie below the V_{crit} curve in Fig. 5; i.e. flow was not of dominant flattening type.

The analysis given above is not meant to be presented as a perfectly reliable method of determining the vorticity number in a naturally deformed sample; it is a first attempt, using rigid-object orientation analysis. The way in which porphyroclasts can change shape during progressive deformation and the effects of fluctuating W_k should be investigated before the method can be more generally applied. It should be clear from this example that populations of rigid objects in ductilely deformed rocks store a significant amount of information, not only on sense of vorticity but also on the vorticity number and deviations from plane strain.

Acknowledgements—Brett Freeman, Subir Ghosh and Chris Mawer offered valuable suggestions for improving the manuscript.

REFERENCES

Bobyarchick, A. R. 1986. The eigenvalues of steady flow in Mohr space. *Tectonophysics* **122**, 35–51.
Bretherton, F. P. 1962. The motion of rigid particles in shear flow at low Reynolds number. *J. Fluid. Mech.* **14**, 284–301.
Freeman, B. 1985. The motion of rigid ellipsoidal particles in slow flows. *Tectonophysics* **113**, 163–183.
Ghosh, S. K. & Ramberg, H. 1976. Reorientation of inclusions by combination of pure and simple shear. *Tectonophysics* **34**, 1–70.
Gierszewski, P. L. & Chaffey, L. E. 1977. Rotations of an isolated triaxial ellipsoid suspended in slow viscous flow. *Can. J. Phys.* **56**, 6–11.
Goldstein, H. 1980. *Classical Mechanics*. Addison-Wesley, London.
Hinch, E. J. & Leal, L. G. 1979. Rotation of small non-axially symmetric particles in a simple shear flow. *J. Fluid Mech.* **92**, 591–608.
Jeffery, G. B. 1922. The motion of ellipsoidal particles immersed in a viscous fluid. *Proc. R. Soc. Lond.* **A102**, 161–179.
Malvern, L. E. 1969. *Introduction to the Mechanics of a Continuous Medium*. Prentice-Hall, Englewood Cliffs, New Jersey.
Means, W. D., Hobbs, B. E., Lister, G. S. & Williams, P. F. 1980. Vorticity and non-coaxiality in progressive deformations. *J. Struct. Geol.* **2**, 371–378.
Passchier, C. W. 1985. Water deficient mylonite zones—an example from the Pyrenees. *Lithos* **18**, 115–127.
Passchier, C. W. 1986. Flow in natural shear zones—the consequences of spinning flow regimes. *Earth Planet. Sci. Lett.* **77**, 70–80.
Passchier, C. W. & Simpson, C. 1986. Porphyroclast systems as kinematic indicators. *J. Struct. Geol.* **8**, 831–843.
Ramberg, H. 1975a. Superposition of homogeneous strain and progressive deformation in rocks. *Bull. geol. Instn. Univ. Uppsala* **6**, 35–67.
Ramberg, H. 1975b. Particle paths, displacement and progressive strain applicable to rocks. *Tectonophysics* **28**, 1173–1187.
Simpson, C. & Schmid, S. M. 1983. An evaluation of criteria to deduce sense of movement in sheared rocks. *Bull. geol. Soc. Am.* **94**, 1281–1288.
Truesdell, C. 1954. *The Kinematics of Vorticity*. Indiana University Press, Bloomington.

APPENDIX

Nomenclature

X_i'	co-ordinates in external reference frame fixed to d_i
X_i	co-ordinates in internal reference frame fixed to OSA
$\dot{X}_i'$	displacement rate—external reference frame
$\boldsymbol{L}'$	velocity gradients tensor—external reference frame
$\boldsymbol{D}'$	symmetric strain rate tensor—external reference frame
$\boldsymbol{W}'$	vorticity tensor—external reference frame
$\boldsymbol{R}$	rotation tensor [Goldstein 1980, eq values (4)–(46)]
$\boldsymbol{d}_i$	eigenvectors of $\boldsymbol{D}'$—instantaneous stretching axes
d_i	eigenvalues of $\boldsymbol{D}'$—instantaneous stretching rates
$\boldsymbol{l}_i$	eigenvectors of $\boldsymbol{L}'$—flow apophyses
$\boldsymbol{v}$	instantaneous displacement rate vector of OSA on a sphere
S	instantaneous stretching factor for plane-strain
W	vorticity
W_k	vorticity number [equation (3)]
$^{\circ}W$	kinematic vorticity number of Truesdell [equation (4)]
β	angle between source and sink in $X_2' - X_3'$ plane [equations (10) and (20)]
a, b, c	length of semi axes rigid object along X_1, X_2, X_3
Mx, Mn	length of long and short semi axes of object in the $X_2' - X_3'$ plane
B_i	Bretherton's shape factors [equation (19)]
B	Bretherton's shape factor for axially symmetric objects [equation (5)]
B^*	ratio long/short axis object in $X_2' - X_3'$ cross-section [equation (20)]
θ, ϕ, ψ	Eulerian angles
$\dot{\theta}, \dot{\phi}, \dot{\psi}$	rate of change of Eulerian angles

ω_i	angular velocities of object around X_i
V	volume change/plane strain deviation factor [equation (14)]
OSA	object symmetry axes

Comparison with other work

Stable positions for ellipsoidal objects in non-coaxial flow have been predicted by previous workers (e.g. Jeffery 1922, Bretherton 1962, Freeman 1985) but the subject has been studied in most detail by Ghosh & Ramberg (1976). They restricted their analysis to a two-dimensional situation, however, and used the addition of pure shear and simple shear (with stretching rates $\dot{\varepsilon}$ and $\dot{\gamma}$, respectively) to obtain a general non-coaxial tensor of displacement rate. Unfortunately this method gives a presentation of $\boldsymbol{L}'$ which unnecessarily complicates the mathematical framework for comparison of flow types with different vorticity numbers: the extensional eigenvector $\boldsymbol{l}_2$ is fixed to one axis of the external reference frame. Freeman (1985) also uses this presentation of $\boldsymbol{L}'$. Ghosh & Ramberg have used $r = a/b$ instead of B and a deviant vorticity number:

$$S_r = \frac{\dot{\varepsilon}}{\dot{\gamma}} \tag{A1}$$

to derive the following equation for angular velocity of a two-dimensional elliptical object in non-coaxial flow:

$$\omega = \frac{\dot{\gamma}\,(r^2 \cos^2\chi + S_r\,(r^2 - 1)\sin^2\chi + \sin^2\chi)}{r^2 + 1}, \tag{A2}$$

where χ describes the orientation of the a axis of the object in the $X_2' - X_3'$ plane. The components of $\boldsymbol{L}'$ and S_r, as used by Ghosh & Ramberg (1976), can be rewritten:

$$S_r = \frac{\sqrt{1 - W_k^2}}{2\,W_k};\quad \dot{\varepsilon} = \frac{S}{2}\sqrt{1 - W_k^2};\quad \dot{\gamma} = W_k S, \tag{A3}$$

if 0, $S/2$ and $-S/2$ are eigenvalues of $\boldsymbol{D}'$ as used in this paper. In this case, for isochoric plane strain flow $W_k = W$. Rewriting r in terms of B, equation (A3) becomes:

$$\omega = \frac{W_k S}{2}(B + 1)\cos^2\chi + \frac{SB}{2}\sqrt{1 - W_k^2}\sin^2\chi + \frac{(1 - B)\,W_k S}{2}\sin^2\chi. \tag{A4}$$

This equation can be simplified by choosing an external reference frame fixed at 45° to $\boldsymbol{d}_i$, the instantaneous stretching axes of the flow:

$$\psi' = \frac{\alpha}{2} - \chi \tag{A5}$$

where $\alpha/2$ is half the angle between $\boldsymbol{l}_2$ and $\boldsymbol{l}_3$ (Bobyarchick 1986, Passchier 1986), related to S and W_k (Fig. 1) by:

$$\cos\alpha = W_k;\quad \sin\alpha = \sqrt{1 - W_k^2}. \tag{A6}$$

Equation (A4) now becomes

$$\omega = \frac{S}{2}(W_k + B\cos 2\psi) \tag{A7}$$

which is equivalent to equation (8) if $\psi = 90°$. In this orientation and for plane strain, the length of the object along the X_2 axis does not influence the equation and this leads to the equivalence with Ghosh & Ramberg's (1976) results for two dimensions or elliptic cylinders with their long axis parallel to the vorticity vector.

The equation relating the critical axial ratio of an object, below which it is permanently rotating, and the vorticity number is given by Ghosh & Ramberg (1976, p. 7) as:

$$r_{crit} = \frac{1 + \sqrt{1 + S_r^2}}{2S_r}.$$

Using B^* and W_k instead of r and S_r this reduces to equation (23):

$$B^*_{crit} = W_k. \tag{A8}$$

The use of a reference frame fixed to $\boldsymbol{d}_i$ (as in this paper) eliminates the need to describe the orientations χ_1 and χ_2 of minimum and maximum velocity of the object as in Ghosh & Ramberg (1976, pp. 10–11), because they are always parallel to X_3' and X_2'. In the reference frame for $\boldsymbol{L}'$ used in this paper, source and sink are symmetrically arranged at an angle $\pm\beta/2$ from X_3', where β is given by equation (10). In Ghosh & Ramberg (1976), both orientations χ_5 and χ_6 suffer an additional rigid body rotation over $\alpha/2$ because of a choice of reference frame fixed to $\boldsymbol{l}_2$ and:

$$\chi_5 = -\frac{\beta}{2} + 90° + \frac{\alpha}{2},\qquad \chi_6 = \frac{\beta}{2} + 90° + \frac{\alpha}{2}. \tag{A9}$$